Mine Water and the Environment (2019) 38:421–430
https://doi.org/10.1007/s10230-018-00584-z

TECHNICAL ARTICLE

Catastrophic Evolution of Water Inrush from A Water-Rich Fault in Front of Roadway Development: A Case Study of The Hongcai Coal Mine

Bo Li[1] · **Qiang Wu**[2]

Received: 15 March 2018 / Accepted: 22 December 2018 / Published online: 4 January 2019

Abstract
A fault can be both the inrush channel and the water source. In order to better understand how such a mine disaster develops, a fluid–solid coupling analysis model and a Forchheimer, nonlinear, non-Darcian flow model were used to study an inrush in the Hongcai coal mine. Numerical simulation was used to reconstruct the dynamic process of the inrush. Then the coupled evolution of the stress, displacement, and seepage fields were analyzed and the precursor information characteristics were summarized. The results showed that the inrush was the result of excavation disturbance and hydraulic pressure in the fault fracture zone. Before the inrush occurs, the stress of the surrounding rock drops after continually increasing, the displacement of the surrounding rock increases sharply after a stable build-up, and the gradually increasing pore water pressure of the surrounding rock decreases rapidly just before the inrush. During this process, the multi-field information in the aquiclude continuously changes. During the inrush, groundwater flows into the roadway from top to bottom along the fault fracture zone. The pressure in the runoff path continuously decreases and the flow velocity generally increases. However, when the water initially enters the channel and roadway, the flow velocity first decreases due to the change in flow direction, and then increases again, and the velocity and pressure gradually stabilizes after the water finally enters the roadway. These results help explain how flooding caused by a water-rich fault inrush evolves and provide a scientific basis for determining the characteristics of appropriate inrush precursors.

Keywords Fluid–solid coupling · Numerical simulation · Precursory information · Dynamic process

Introduction

Coal accounts for about 70% of China's primary energy production and consumption and will continue to be China's major energy source for a long time. However, the hydrogeological conditions in China's coalfields are very complicated. There are various water hazards and frequent water inrush accidents (Qian and Shi 2003; Wu 2014; Wu et al. 2016; Zhang et al. 1997). According to water inrush statistics, 80% of such accidents are related to faults (Li et al. 2018; Santos and Bieniawski 1967). Li et al. (1996) divided the faults into open and closed types and concluded that the mechanism of water inrush of an open fault is caused by the opening of the walls by the force of the confined water. For a closed fault to be the cause, destruction of the walls or an area of weakness must be present at a key part of the fault.

Bu and Mao (2009) focused on mining's mechanical characteristics and water inrush through large faults above or below the coal seam, and established a mechanical model for analyzing the mechanism of fault activation at the bottom of a stope, and obtained the stress field distribution of faulted rocks at different depths. Pu and Zhang (2010) simulated the distribution of stress and plasticity of surrounding rock for a coal seam under an unconsolidated aquifer in situations with and without a fault, revealing the mechanism of formation of water inrush through the mine roof. Bense et al. (2003) used digital-image analysis to study the spatial distribution, deformation mechanism, and hydraulic characteristics of water conductivity around the fault zone. Nelson et al.

✉ Bo Li
libo1512@163.com

[1] Key Laboratory of Karst Environment and Geohazard, Ministry of Land and Resources, Guizhou University, Guiyang 550000, Guizhou, China

[2] National Engineering Research Center of Coal Mine Water Hazard Controlling, China University of Mining and Technology (Beijing), Beijing 100083, China

(1999) analyzed the fluid characteristics of the material in a fault zone and concluded that the hydraulic activity of the medium is greatly enhanced by fractures in the fault zone, which may not be obvious. Wu et al. (2008) introduced the main controlling factors of lagging water inrush at the fault, and put forward the concept of the weakening effect of time on a fault in the coal seam floor.

These studies can be used to explain the nature of most fault-related inrush events where the fault acts as a conduit of water from an aquifer or aquifers. However, cases where the fault acts as both the water conduit and is the only inrush water source are still extremely unpredictable, sudden, and harmful. In addition, due to the particularities of the underlying hydrogeological conditions, the mechanism of such events is significantly different from those of other types of water inrush. Given this, the water inrush event that occurred in the 1301 air return way of the Hongcai coal mine in 2016 was used as a case study, and the dynamic process of water inrush at the front-lying fault in the roadway was reproduced by numerical simulation. The evolution of the stress, seepage, and displacement fields, and the precursory information characteristics of the water-rich fault were analyzed; the results provide a scientific basis for the interpretation, monitoring, and early warning of water inrush at such a fault.

Project Overview

The designed production capacity of the Hongcai coal mine is 30 million t/a. The mine is located in Shaomi Village, Shuicheng County of Guizhou Province, about 24 km southwest of Liupanshui City. The overall topography is low in the southwest and high in the northeast, with an elevation of 399 m. The strata in the area are (from newest to oldest): the Quaternary, the lower Triassic Feixianguan Formation, the upper Permian Longtan Formation, and the Emeishan Basal Formation. The main coal seam is located in the Longtan Formation, with a coal thickness of 2–4 m and an inclination of 8°–10°. The geological structure of the area is located in the west wing of a northwest trending deformation zone on the Yangtze platform, with a monoclinic structure and a northeastern tendency. The study area belongs to the Bala River basin of the Pearl River system. Since the surface water system is not developed, the area mainly relies on atmospheric precipitation for water. Due to the terrain, water in the study area is generally recharged from and drained to nearby regions. Fissure water in the clastic rock structures in the area is also supplemented by atmospheric precipitation, and the groundwater dynamics vary significantly across seasons. Generally, the groundwater flow and water level start to rise in May each year and increase to peaks in June to September, with 1–3 peaks during the period. Then the water level and flow rate gradually decrease from October to December, with its lowest point coming in April (Fig. 1).

In July 2016, a water inrush accident occurred in the 1301 air return way of the Hongcai coal mine when it was developed to 438 m. The total water inflow was about 4200 m^3 and the duration was 4 h. After the disaster, it was discovered that a water-rich fault in the development region of the 1301 air return way was the main cause of the accident; the fault was both the inrush channel and the source of the inrush water. Atmospheric rainfall flows along the surface depression of the fault, infiltrates into the fault zone over long period of time, and accumulates there. The fault inclination was 216°, the dip angle was 69°, and the fault separation was 10 m. The lithology of the strata cut by fault is mainly consisted of claystone, siltstone, fine sandstone, and the coal seam. The fracture development degree and water content of both walls of the fault were poor.

Fluid–Solid Coupling Analysis of Water Inrush from A Water-Rich Fault

Mathematical Model of Fluid–Solid Coupling

Assuming that the rock mass is a porous medium, and the fluid in the rock mass flows based on Darcy's law and Biot fluid–solid coupling equation, i.e.:

$$\begin{cases} G\nabla^2 u_j - (\lambda + G)\frac{\partial \varepsilon_v}{\partial x_j} - \frac{\partial p}{\partial x} + f_j = 0 \\ K\nabla^2 p = \frac{1}{S}\frac{\partial p}{\partial t} - \frac{\partial \varepsilon_v}{\partial t} \\ \varepsilon_v = -\left(\left(\frac{\partial u_x}{\partial x}\right) + \left(\frac{\partial u_y}{\partial y}\right) + \left(\frac{\partial u_z}{\partial z}\right)\right) \end{cases}, \quad (1)$$

where λ and G are the Lame constants, p is the pore water pressure, ε_v is the bulk strain, x_j is the coordinate of in direction j, u_j is the displacement in direction j, f_j is the bulk force in direction j, K is the coefficient of permeability, ∇ is the Labrador operator, S is the elastic storativity, $\partial p/\partial x_j$ is the influence of seepage on the rock mass skeleton, and $\partial \varepsilon_v/\partial t$ is the influence of rock mass strain on seepage.

Equation 1 does not consider the effect of rock mass deformation on the coefficient of permeability and the factor of porosity. In previous studies, researchers generally considered these parameters as constants for model simplification. However, when the rock is under stress, its coefficient of permeability and factor of porosity will change as the stress–strain changes (Peng et al. 2003). Equation 2, based on the permeability and porosity control equations (Elsworth and Bai 1992; Rutqvist and Tsang 2002), was programmed into the calculation model so that the permeability and porosity of the surrounding rock could be synchronized

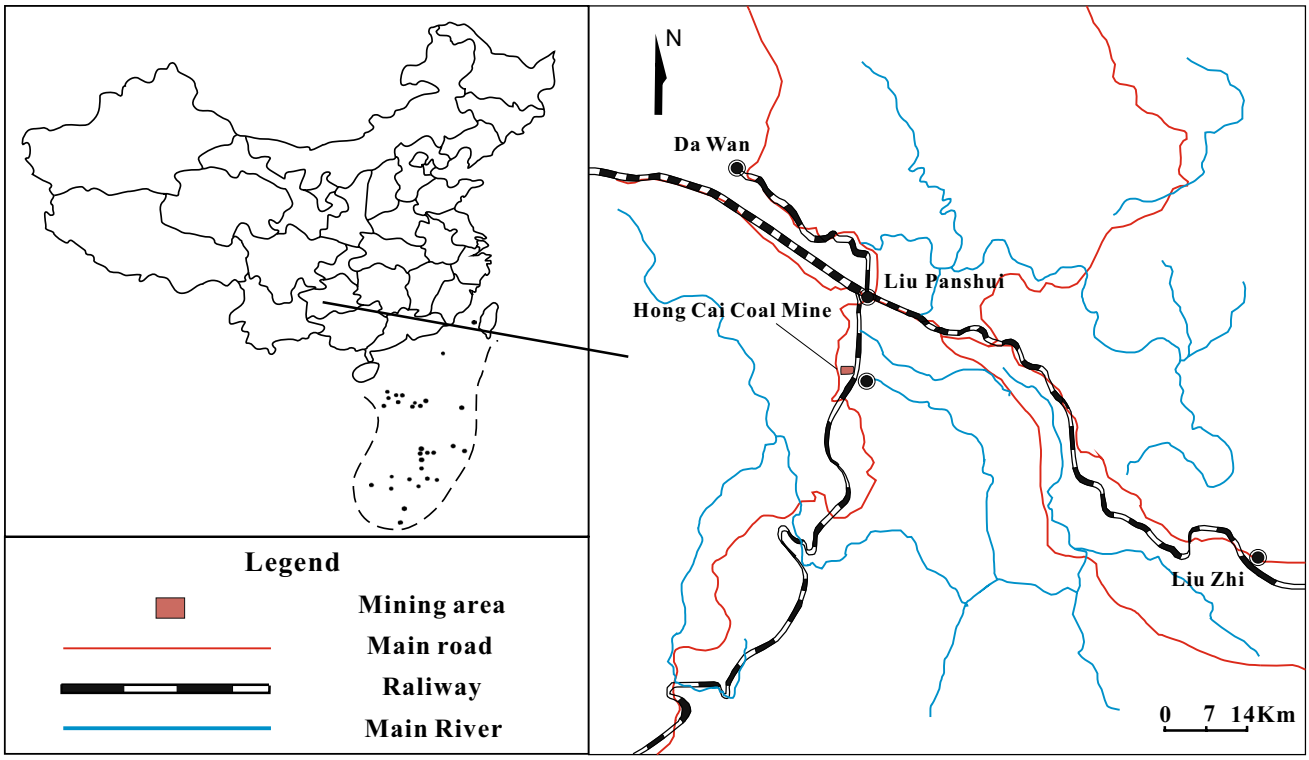

Fig. 1 Traffic and location

with the deformation of rock mass to simulate the water inrush more accurately.

$$\begin{cases} \sigma = \left(\phi_0 - \phi_r\right)\exp(-\alpha_\phi \cdot \overline{\delta_v}) + \delta_r \\ \overline{\delta_v} = \frac{(\delta_1+\delta_2+\delta_3)}{3} - \alpha p \\ K = K_0\left(\frac{1+\Delta\varepsilon}{\phi}\right)^2 \end{cases} . \tag{2}$$

In Eq. 2, Φ_o is the initial factor of porosity, Φr is the extreme value of the factor of porosity, α_Φ is the stress influence coefficient and can take the value of 5×10^{-8} Pa, α is the Biot effective stress coefficient, δ1, δ2, and δ3 are the three principal stresses, K_0 is the initial coefficient of permeability, and $\Delta\varepsilon$ is the change in bulk strain.

Numerical Calculation Model

Based on the actual geologic conditions of the development face of the 1301 air return way, a Mohr–Coulomb constitutive model (Fig. 2) was established. The model dip angle was 10°, the fault dip angle was 60°, and the fault zone width was 10 m. The development face in the sandstone formation lay over the coal seam. The development process was divided into 19 time intervals. During the first 11, mining advances by 4 m, while during the remaining eight intervals, as mining approaches the fault fracture zone, it advances by 2 m. Monitoring points of displacement and maximum shear strain were set at the top and bottom of the roadway as well as around the fault. The mechanical boundary conditions of the model were: fully constrained boundary conditions were used for the bottom, free boundary conditions were used for the top of the model, and fixed boundaries in the x-direction were adopted at the left and right side of the model. The boundary conditions for seepage were: the left, right, and bottom of the fault fracture zone were impermeable boundaries; a 4 m head was set at the top of the fault fracture zone according to the measured water level of the depression before the water inrush; the initial hydrostatic pressure inside the fault fracture zone was estimated according to $p=\rho gh$ (P is the water pressure; ρ is liquid density; g is the unit of gravity, which is 9.8 N/kg; and h is the height of the water surface from any location in the fault zone to the depression); and the initial coefficient of permeability in the fault fracture zone was 1.2×10^{-10} m^2/Pa s. The mechanical parameters of the rock strata are listed in Table 1.

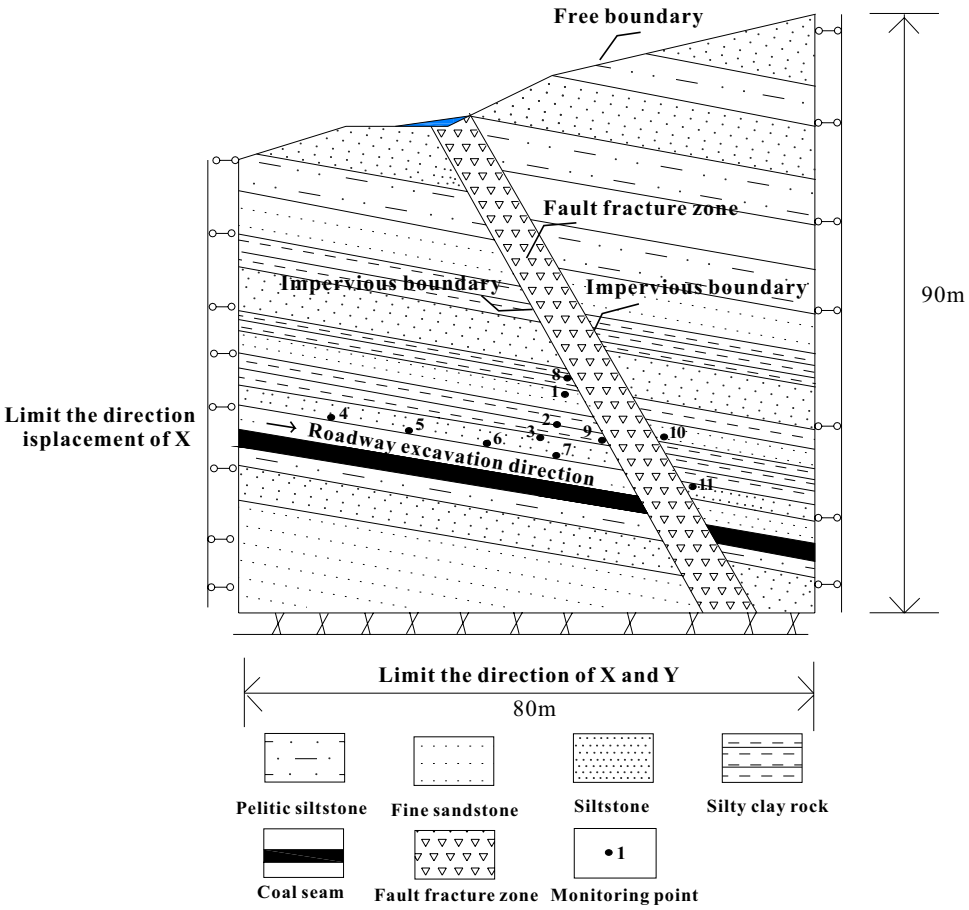

Fig. 2 Numerical calculation model

Table 1 Mechanical parameters of rock mass

Rock stratum	Bulk modulus (MPa)	Shear modulus (MPa)	Poisson ratio	Angle of internal friction (°)	Cohesion (KPa)	Tensile strength (KPa)	Density ($Kg{\cdot}m^{-3}$)
Silty clay rock	4730	3550	0.2	47	900	1100	2650
Pelitic siltstone	2400	1730	0.21	45	500	640	2510
Siltstone	4950	4350	0.16	50	1000	930	2600
Coal seam	1670	770	0.3	32	450	420	2400
Fine sandstone	4800	4220	0.17	48	980	1200	2500
Fault fracture zone	1500	780	0.28	30	500	550	2200

Numerical Calculation Results and Analysis

Stress Field of The Surrounding Rock

Figure 3 shows the simulated stress field of the surrounding rock when the developing face is located at different distances from the fault. It can be seen that the stress redistribution caused by the development disturbance causes the stress concentration at both ends of the roadway to increase and that the stress in the fault fracture zone is less than in the surrounding rock. The fault fracture zone is the relative pressure relief zone, and the stress concentration in the developing face near the fault is less than that on the other side of the roadway. As the developing face advances, the stress in the rock surrounding the face increases and decreases, and deforms (compressing and expanding), which causes pull and shear failure. This corresponds to the change in maximum shear strain measured by the sensor in the roof of roadway (Fig. 4). The maximum shear strain initially increases and then decreases, and then the maximum shear strain of plastic surrounding rock, which has been deformed and destroyed under the system adjustment, increases again. Characteristics of the stress change collected by the sensor can be generalized into a slow increase at a development

distance L ≤ 2 4 m, a rapid increase at 24 m ≤ L ≤ 52 m, and a rapid decrease at L ≥ 52 m.

Displacement Field of The Surrounding Rock

Figure 5 shows the simulated vertical displacement of the surrounding rock during development. It can be seen that the redistribution of the displacement field caused by the development disturbance causes the roadway roof be displaced downward, whereas the bottom moves upward. As mining progresses, the displacement increases continuously. When the developing face is further from the fault, the vertical negative displacement in the fault fracture zone is less than in the surrounding rock, and the fracture zone is the relative reduction zone. The closer the developing face is to the fault fracture zone, the less obvious is this phenomenon.

As shown by the curves observed by monitoring points in Figs. 6 and 7, the vertical displacement at the roof and the bottom wall of the fault generally increases as the developing face advances. The displacement characteristics can be generalized into a moderately increased area at a development distance L ≤ 24 m, a rapid increase in area at

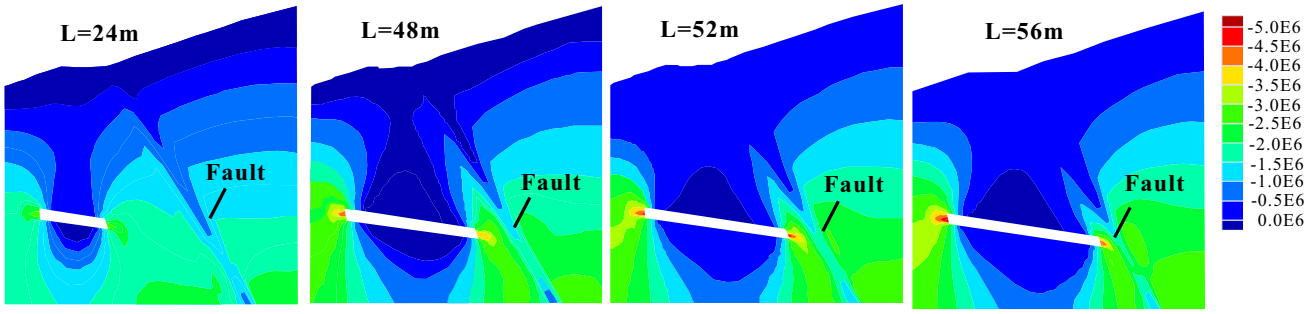

Fig. 3 Distribution map of stress field of surrounding rock at different development distance

Fig. 4 Maximum shear strain change curve at the roadway roof monitoring points

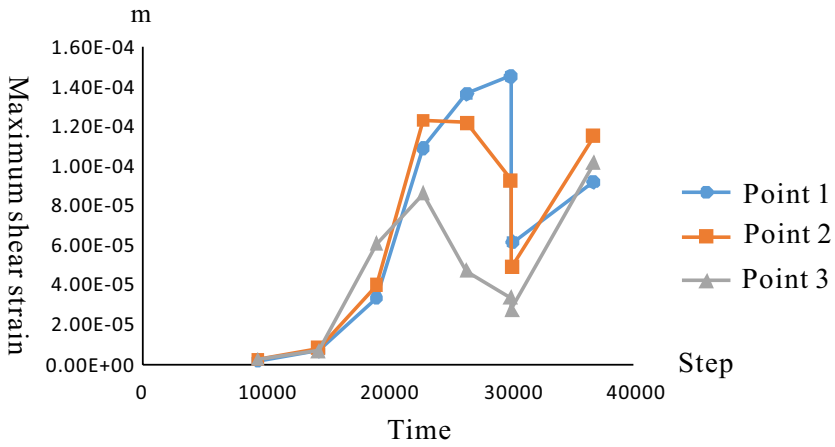

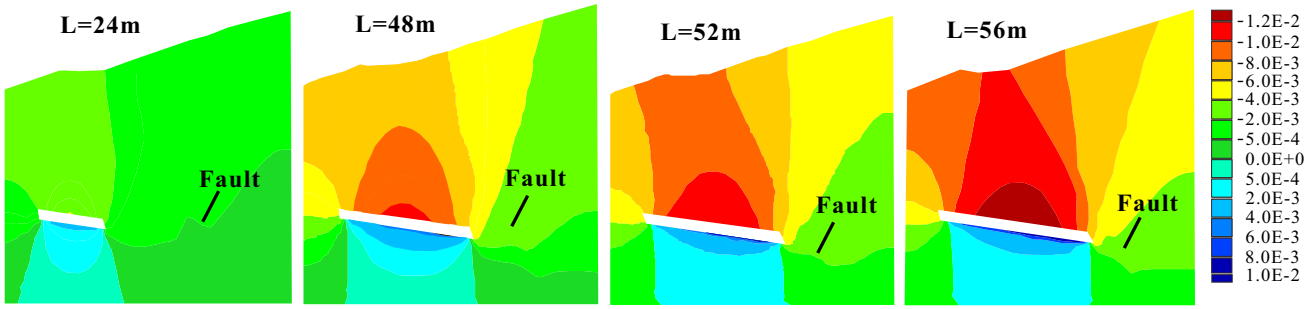

Fig. 5 Distribution map of displacement field of surrounding rock at different development distance

24 m ≤ L ≤ 52 m, and a sharp increase in area at L ≥ 52 m. Impact at the observation spots in the upper section of the fault is relatively low since the observation spots are separated from the developing face by the fault fracture zone.

Plastic Zone of The Surrounding Rock

Figure 8 shows the simulated deformation of the plastic zone in the surrounding rock at different distances between the developing face and the fault. It can be seen that as mining advances, the plastic zone of the surrounding rock near the fault increases continuously. When the development distance, L = 48 m, isolated damage zones are formed in the transition area from the development face to the fault fracture zone. When L = 52 m, the isolated damage zones in the transition area further enlarge. When the distance increases to L = 56 m, the damaged zones between the fault fraction zone and development

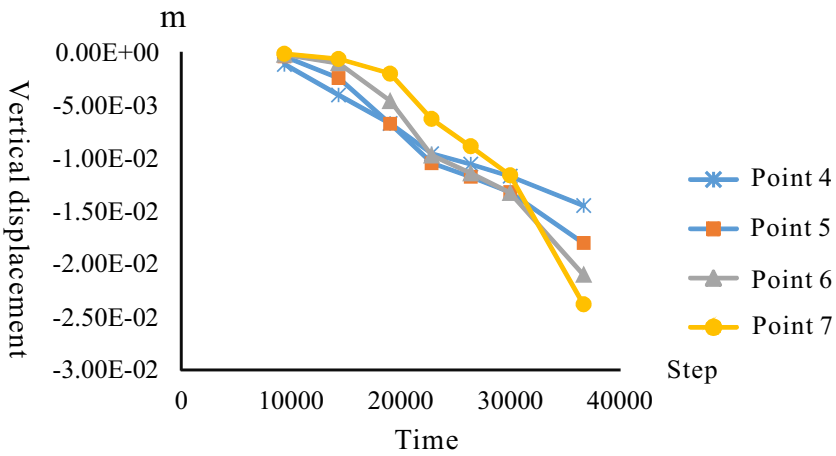

Fig. 6 Vertical displacement change curve of roadway roof monitoring points

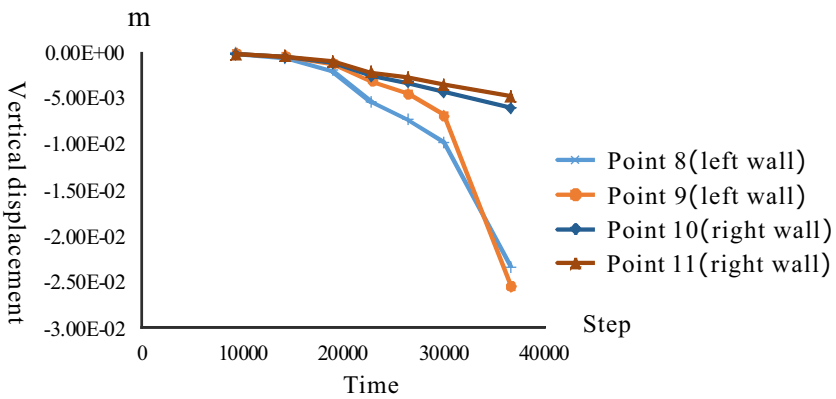

Fig. 7 Vertical displacement change curve of two walls of fault monitoring points

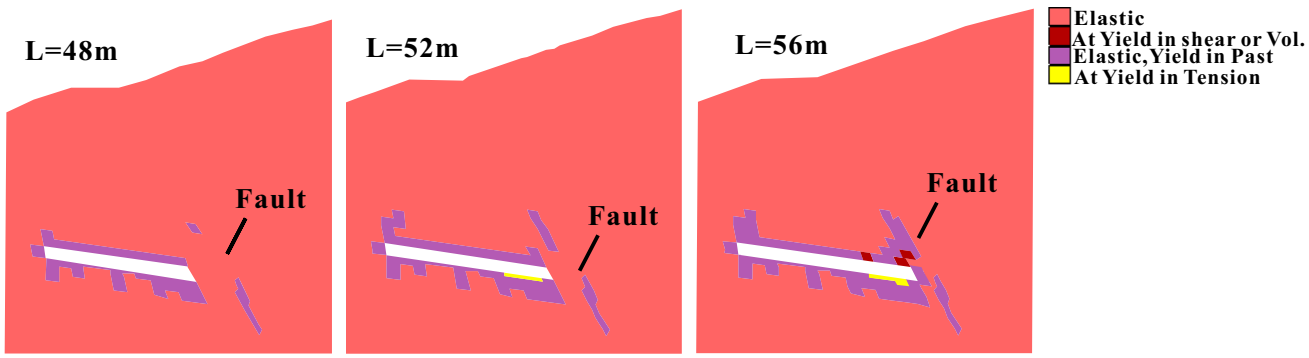

Fig. 8 Distribution of plastic zone of surrounding rock at different development distance

face connect; it is very likely that a water inrush accident will occur at this time.

Pore Water Pressure of the Surrounding Rock

Figure 9 shows the simulated pore water pressure changes at different distances from the fault to the developing face. It can be seen that at a development distance, L = 24 m, the disturbance has no obvious effect on the pore water pressure in the fault. When the distance increases to L = 48 m, the pore water pressure in the lower part of the water-rich fault increases significantly. When the distance increases to L = 52 m, the pore water pressure continues to increase slowly. When the distance increases to L = 56 m, the pore water pressure in the fault decreases rapidly; at this time, the damaged zones between the fault zone and the development face are connected. The pore water pressure changes near the fault is consistent with the change of stress in the aquitard.

Analysis of the Seepage Process of Water Inrush at Water-Rich Fault

Non-Linear Seepage Coupling Model

Recent studies generally indicate that the seepage of fractured rock does not follow Darcy's law, but follows the Forchheimer nonlinear seepage equation (Pradipkumar and Venkataraman 1995; Ma et al. 2016; Shi et al. 2016). The fault fracture zone in the study area is poorly cemented, and the particles are large, contributing to a high porosity. After the water inrush channel is formed, the flow velocity at the fault fracture zone will significantly increase, and the nonlinear characteristics of the seepage is obvious, which is suitable for using the Forchheimer equation. When water inrush occurs, the flow of groundwater in the roadway is turbulent, which is suitable for the Navier–Stokes equation of viscous Newtonian fluid flow. In this study, the groundwater flow in these two regions are combined together. Comsol Multiphysics, the multi-physics coupling simulation software, was used to analyze the seepage field runoff in the water inrush. In the numerical model, the fluid density is 1000 kg/m^3 and the dynamic viscosity is 1×10^{-3}N s/m^2. The top of the fault fracture zone is the fixed water head boundary, and the pressure of water near the junction with the roadway is 0.52 MPa. The remaining boundaries are treated as impermeable. Other parameters of the model are listed in Table 1. The momentum equations of groundwater at the different stages are:

1. Non-Darcy Forchheimer seepage at the fault fracture zone

$$\begin{cases} \frac{\rho}{\phi}\left((u\cdot\nabla)\frac{u}{\phi}\right) = \nabla\left[-pI+\frac{\eta}{\phi}\left(\nabla u+(\nabla u)^T\right)\right]-\left(\frac{\eta}{K}+\beta_F|u|+Q\right)u+F \\ \rho\nabla\cdot u = Q \end{cases}. \tag{3}$$

2. Navier–Stokes turbulence in the roadway

$$\begin{cases} \rho u\cdot\nabla u = \nabla\cdot\left(-pI+\eta(\nabla u+\nabla u)^T\right)+F \\ \nabla\cdot u = 0 \end{cases}, \tag{4}$$

where u is the fluid velocity, K is the permeability, η is the kinematic viscosity, P is the fluid pressure, ρ is the fluid density, F is the fluid resistance (related to gravity and fluid compressibility), I is the identity matrix, Q is the source (sink) strength, Φ is porosity, and β_F are the drag parameters $\beta_F = \frac{\rho\varphi C_f}{\sqrt{k}}\left(C_f = \frac{1.75}{\sqrt{150\phi^3}}\right)$.

Numeric Calculation and Analysis

Figures 10 and 11 show the velocity and pressure distribution when groundwater flows from the non-Darcy Forchheimer area at the fault fracture zone to the Navier–Stokes turbulence in the roadway. It can be seen from Fig. 10 that

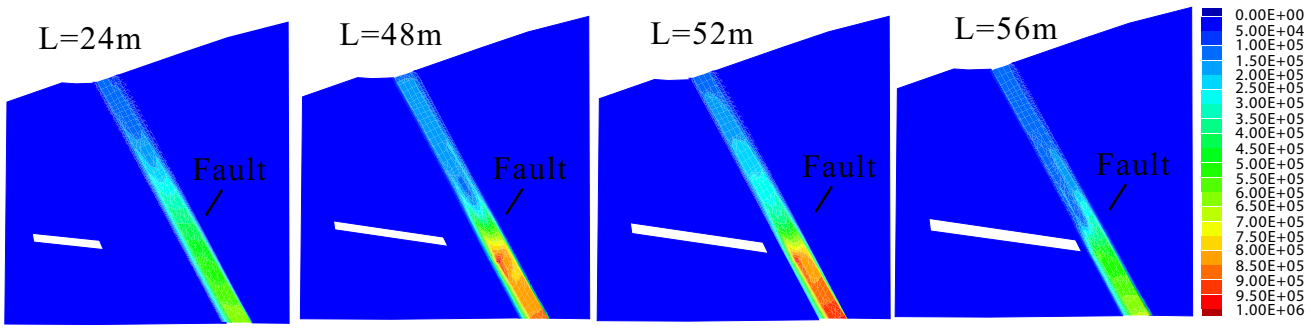

Fig. 9 Distribution of pore water pressure at different development distances

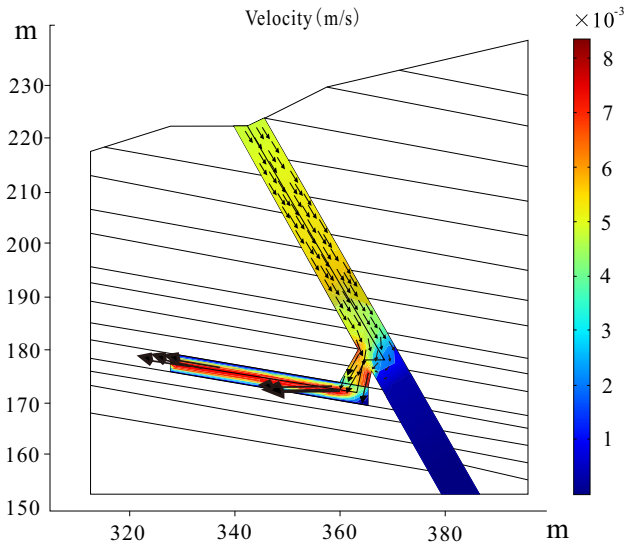

Fig. 10 Distribution of flow velocity on the flow path

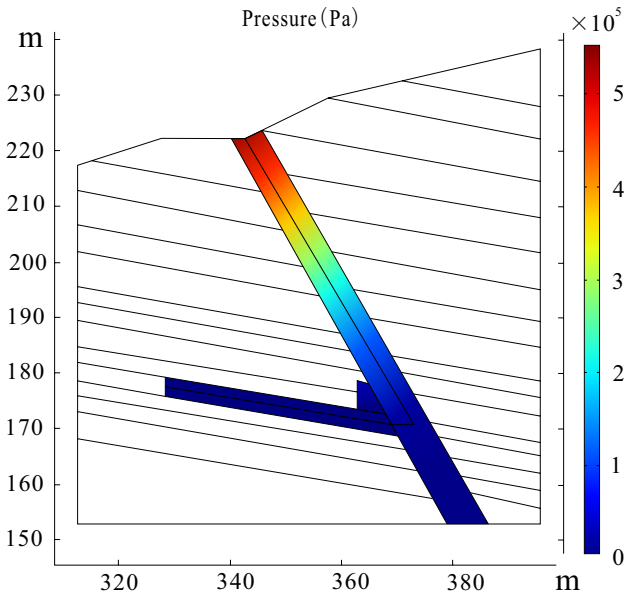

Fig. 11 Distribution of water pressure on the flow path

the velocity generally increases during the flow, increasing slightly from the top of the fault fracture zone to its upper section, and greatly increasing in the water inrush channel and roadway. The pressure reaches a low value near the interface between the fault fracture zone and water inrush channel. This is because water flows into the roadway and transforms pressure into kinetic energy, resulting in a sharp drop in pressure.

Figures 12 and 13 record the changes in flow velocity and pressure observed at each sensor. In the Forchheimer area, the velocity from the top of the fault to its upper section increases slightly from 4.2×10^{-3} m/s to 5.5×10^{-3} m/s (Fig. 12). At the junction of the fault and inrush point, the flow velocity obviously decreases and fluctuates from 5.5×10^{-3} m/s to 4.0×10^{-3} m/s. This is due to the change of flow direction at this point, since kinetic energy is consumed to overcome the friction between water molecules. After the groundwater enters the inrush channel, the flow velocity increases sharply, from 4.0×10^{-3} m/s to 8.3×10^{-3} m/s. The groundwater flow velocity decreases again at the outlet of the inrush channel, from 8.3×10^{-3} m/s to 5.0×10^{-3} m/s, After entering the roadway, the groundwater flow is turbulent and the flow rate increases to 1.0×10^{-3} m/s and then remains stable. The pressure decreases throughout the process (Fig. 13), from the top of the fault to the inrush channel, the pressure decreases rapidly, from 0.52 MPa to 0.16 MPa. When the fluid enters the inrush channel, the pressure decreases slowly, from 0.15 MPa to 0.1 MPa. When the fluid enters the roadway, the pressure stabilizes.

Conclusion

Using the water inrush event in the Hongcai coal mine as a case study, numerical simulation was used to reproduce the changes in the stress, displacement, and seepage fields of the surrounding rock during the formation, development, and occurrence of the water inrush. The results show that the inrush from the water-rich fault was the result of excavation disturbance and hydraulic pressure in the fault fracture zone.

The model indicates that the roadway and nearby rock were likely damaged in the early stage of excavation and disturbance, causing fissures to start to appear in the aquitard. The stress, displacement, and seepage in the surrounding rock all increased steadily. When the developing face approached the water-rich fault, the damaged area expanded further. The internal fractures in the water-bearing layer and surrounding rock began to expand locally, and water pressure was also transmitted. The multi-field information data of the water-barrier and fault zone then rapidly increased. With the continued advancement of the developing face, a wide range of damaged areas were formed, and the aqueduct gradually cracked. When the developing face advanced to the critical value, multiple fields of the rock surrounding the aqueduct suddenly failed and the surrounding rock became unstable, causing the water to rush in. As a whole, the aquifer's multi-field information can be divided into three stages: the initial change when the developing face was far from the fault, and then faster changes, and then an abrupt change as the mining approached the fault.

During the inrush, groundwater rushed into the roadway from top to bottom along the fault fracture zone. The pressure in the runoff continuously decreased and the flow velocity generally increased. However, the flow direction

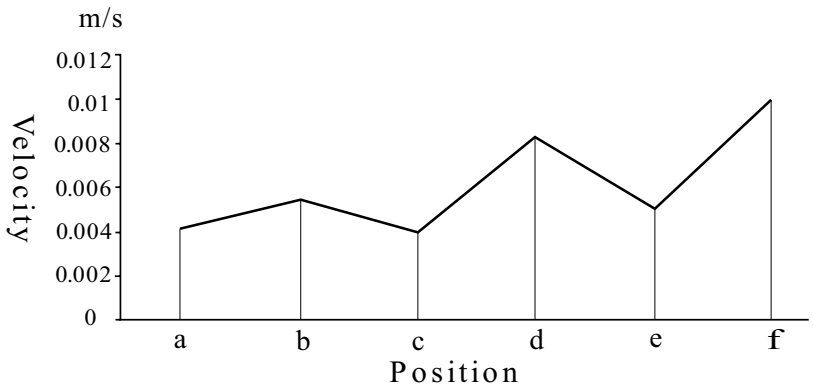

Fig. 12 Flow velocity at each monitoring points

(a: Top of fault; b: Upper part of fault; c: Entrance of water inrush channel; d: Inside of water inrush channel; e: Outlet of water inrush channel; f: Inside roadway)

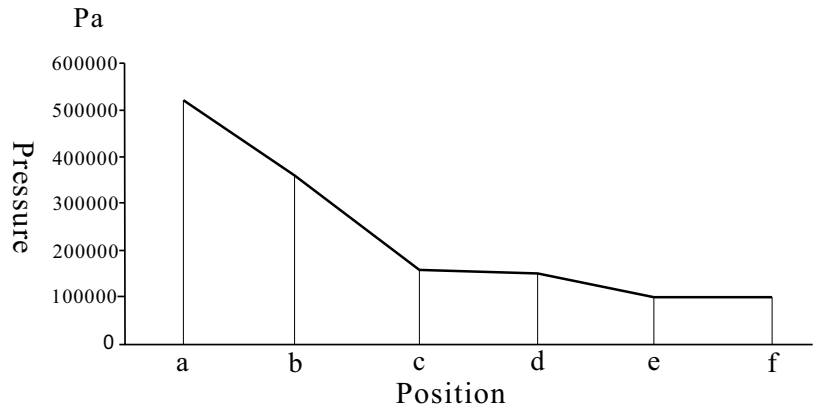

Fig. 13 Water pressure at each monitoring points

(a: Top of fault; b: Upper part of fault; c: Entrance of water inrush channel; d: Inside of water inrush channel; e: Outlet of water inrush channel; f: Inside roadway)

changed as the water flowed from the inrush channel into the roadway, so the flow rate decreased significantly, and then increased again. The flow rate and pressure gradually stabilized after the water entered the roadway.

Through our analysis of the inherent relationships contained within the multi-field information and its effectiveness in predicting the water inrush from the water-rich fault, it is clear that relatively obvious precursory features existed before the water inrush event. Before the aquiclude rupture induced the water inrush, the stress in the surrounding rock fell after continually increasing, while the displacement of the surrounding rock increased sharply, and the amount of vertical negative displacement inside the fault fracture zone decreased. The pore water pressure in the surrounding rock significantly increased near the fault, but decreased rapidly just before the water inrush. This information can be used as a precursor for monitoring and early warning of an inrush from a water-rich fault, and provides a scientific basis for the prevention and control of such events.

Acknowledgements This research was financially supported by the China National Natural Science Foundation (Grants 41702270, 41572222, and 41702261), Guizhou University Introducing Talents Research Foundation (2014-61), Guizhou Province Science and Technology Planning Project (Qian Ke He Platform Talent [2017]5788), Guizhou Provincial Education Dept. Youth Science, and the Technology Talent Growth Project (Qian Jiao He KY Zi [2018]113), Guizhou Provincial Basic Research Program Key Project (Qian Ke He Ji Chu [2019]1413).

References

Bense VF, Berg EHVD, Balen RTV (2003) Deformation mechanisms and hydraulic properties of fault zones in unconsolidated sediments; the Roer Valley rift system, The Netherlands. Hydrogeol J 11(3):319–332

Bu WK, Mao XB (2009) Research on effect of fault dip on fault activation and water inrush of coal floor. Chin J Rock Mech Eng 21(2):119–123

Elsworth D, Bai M (1992) Flow-deformation response of dual-porosity media. J Geotech Eng 118(1):107–124

Li LJ, Qian MG, Li SG (1996) Mechanism of water-inrush through fault. J Chin Coal Soc 21(2):119–123 (in Chinese)

Li B, Wu Q, Duan XQ, Chen MY (2018) Risk analysis model of water inrush through the seam floor based on set pair analysis. Mine Water Environ 37(4):281–287

Ma D, Bai HB, Miao XX, Pu H, Jiang BY, Chen ZQ (2016) Compaction and seepage properties of crushed limestone particle mixture: an experimental investigation for Ordovician karst collapse pillar groundwater inrush. Environ Earth Sci 75(1):1–14

Nelson EP, Kullman AJ, Gardner MH, Batzle M (1999) Fault-fracture networks and related fluid flow and sealing, Brushy Canyon formation, west Texas. In: Haneberg WC, Mozley PS, Moore JC, Goodwin LB (eds) Faults and Subsurface Fluid Flow in the Shallow Crust, 113. AGU, Washington, pp 69–81

Peng SP, Meng ZP, Wang H, Ma CL, Pan JN (2003) Experimental study on pore ratio and permeability of sandstone under different confining pressures. Chin J Rock Mech Eng 22(5):742–746 (in Chinese)

Pradipkumar GN, Venkataraman P (1995) Non-darcy converging flow through coarse granular media. J Inst Eng (India) 76:6–11

Pu H, Zang J (2010) Numerical simulation of water inrush from coal roof affected by fault. J Min Saf Eng 27(3):421–424 (in Chinese)

Qian MG, Shi PW (2003) Mining pressure and strata control. Univ of Mining and Technology of China Press, Xuzhou (in Chinese)

Rutqvist J, Tsang CF (2002) A study of caprock hydromechanical changes associated with CO_2-injection into a brine formation. Environ Geol 42:296–305

Santos CF, Bieniawski ZT (1967) Floor design in underground coalmines. Rock Mech Rock Eng 22(4):249–271

Shi WH, Yang TH, Liu HL, Yang B, Yang X, Zhou YF (2016) Non-darcy flow model and numerical simulation for water-inrush in fractured rock mass. Chin J Rock Mech Eng 35(3):446–455 (in Chinese)

Wu Q (2014) Progress, problems and prospects of prevention and control technology of mine water and reutilization in China. J Chin Coal Soc 39(5):795–805 (in Chinese)

Wu Q, Zhu B, Li JM, Hong YQ, Qian ZJ (2008) Numerical simulation of lagging water-inrush mechanism of rock road ways near fault zone. J China Univ Min Technol 37(6):421–424 (in Chinese)

Wu Q, Li B, Chen YL (2016) Vulnerability assessment of groundwater inrush from underlying aquifers based on variable weight model and its application. Water Resour Manag 30(10):3331–3345

Zhang JC, Zhang YZ, Liu TQ (1997) Rock mass permeability and coal mine water inrush. Geological Publ Press, Beijing (in Chinese)